Effect of Advection by Upper-Tropospheric Background Zonal Wind on MJO Phase Speed

PAUL E. ROUNDY^a

^a University at Albany, State University of New York, Albany, New York

(Manuscript received 11 November 2021, in final form 15 March 2022)

ABSTRACT: A robust linear regression algorithm is applied to estimate 95% confidence intervals on the background wind associated with Madden–Julian oscillation (MJO) upper-tropospheric atmospheric circulation signals characterized by different phase speeds. Data reconstructed from the ERA5 to represent advection by the upper-tropospheric background flow and MJO-associated zonal wind anomalies, together with satellite outgoing longwave radiation anomalies, all in the equatorial plane, are regressed against advection data filtered for zonal wavenumber 2 and phase speeds of 3, 4, 5, and 7 m s⁻¹. The regressed advection by the background flow is then divided by the negative of the zonal gradient of regressed zonal wind across the central Indian Ocean base longitude at 80°E to estimate the associated background wind that leads to the given advection. The median estimates of background wind associated with these phase speeds are 13.4, 11.2, 10.5, and 10.3 m s⁻¹ easterly. The differences between estimated values at neighboring speeds suggests that advection acts most strongly in slow MJO events, indicating that the slowest events happen to be slow because they experience stronger easterly advection by the upper-tropospheric background wind.

SIGNIFICANCE STATEMENT: The Madden–Julian oscillation (MJO) is the dominant subseasonal rainfall signal of the tropical atmosphere. This project shows that the background wind of the tropical atmosphere most especially slows down the slowest MJO events. Understanding what controls its speed might help scientists better predict events.

KEYWORDS: Madden-Julian oscillation; Subseasonal variability; Tropical variability

1. Introduction

Although convection and atmospheric circulation signals associated with the Madden-Julian oscillation (MJO; Madden and Julian 1972) are often reported as moving eastward at near 5 m s⁻¹, events propagate over a wide range of phase speeds. Several different factors could influence the eastward phase speed, including wave dynamics, moist processes, and advection by the background flow (Suematsu 2018; Roundy 2021; Suematsu and Miura 2020). Understanding the factors that influence MJO propagation may help us improve its simulation and prediction. Several authors have recently discussed the phase speed of the MJO. Chen and Wang (2020) found that faster MJO events that have stronger lower-tropospheric Kelvin wave easterly wind signals to the east of the active convection, and that in a simple model, this signal is associated with higher sea surface temperature in the central equatorial Pacific region. However, some observations suggest that the MJO signal often slows down over the west and central Pacific as El Niño signals emerge (e.g., Gribble-Verhagen and Roundy 2010). Hu and Li (2021) show that MJO events that have upward motion anomalies that tilt more strongly with height propagate eastward more rapidly. The implied correlation between tilt and phase speed was near 0.5, suggesting that this mechanism might explain 25% of the variance in phase speed.

Openotes content that is immediately available upon publication as open access.

Corresponding author: Paul E. Roundy, proundy@albany.edu

Using an aquaplanet model, Jiang et al. (2020) suggest that MJO phase speed is strongly modulated by the zonal gradient of lower-tropospheric humidity, and that differences in the mean moisture gradients in models may explain differences in the statistics of MJO phase speed between the models. These works leave open the potential for direct effects of low-frequency background wind circulations on MJO phase speed.

The MJO is thought to dominate a region of the power spectrum centered around periods of 48 days and spread over wavenumbers 0-5 or higher eastward (Wheeler and Kiladis 1999). Power in different parts of the spectral peak comes from different propagation characteristics of the MJO in different parts of the world. For example, when convection is active over the Indian or west Pacific Oceans, wavenumber 2 dominates (e.g., Hendon and Salby 1994; Roundy 2018; also, consider how active or suppressed convection over the Indian Ocean typically cooccurs with the opposite over the west Pacific, all west of 180° longitude). Over the Indo-Pacific warm pool regions, signals associated with the MJO tend move slowly. In contrast, as they enter the Western Hemisphere, with some exceptions (e.g., Gribble-Verhagen and Roundy 2010), they speed up and broaden zonally so that they project there onto wavenumber 1. The power spectral peak of outgoing longwave radiation, precipitable water, and rainfall data (e.g., Wheeler and Kiladis 1999; Cho et al. 2004) at near 48 days implies that signals at both longer and shorter periods achieve lower spectral power. Approaching the spectral peak at 48 day periods from shorter periods, the slower speeds implied are associated with higher amplitudes in the analyzed variables associated with rainfall rate. However, at

DOI: 10.1175/JAS-D-21-0298.1

periods longer than 48 days, slower phase speeds imply less average amplitude in rainfall-associated quantities. So average rainfall intensity cannot be the only factor potentially controlling phase speed, because above or below 48 days, the same average rain rate must be associated with two phase speeds, one higher and one lower than 4–5 m s⁻¹. If higher rainfall rates did strictly slow the MJO, all else being equal, there would be no spectral peak (the spectrum would just be red). Moist coupling might slow the MJO down, but some other explanation would then be needed for reduced amplitude at periods longer than 48 days. Shaaban (2020; A. Shaaban 2021, personal communication) recently showed that higher background lower-tropospheric humidity over Africa, the Indian Ocean, and the Maritime Continent is associated with faster MJO propagation through the same regions. He suggested that this result may not be caused by differences in moist processes, but instead by correlated quantities. He showed that higher levels of lower-tropospheric moisture over Africa east to the Maritime Continent is associated with anomalous lowertropospheric easterly wind and upper-tropospheric westerly wind. The lower-tropospheric humidity is increased in that setting by the more easterly low-level background flow, acting on an eastward humidity gradient. He suggested the hypothesis that variability in upper-tropospheric zonal wind may dominate variability in the phase speed of the MJO, instead of moist physics. Upper-tropospheric background wind is chosen as the focus of this manuscript because it varies with substantially greater amplitude than lower-tropospheric wind, and so will more substantially influence the variability of the phase speed of MJO-associated circulation (the standard deviation of 100-day low-pass filtered ERA5 wind at 80°E and the equator at 200 hPa is 6 times that at 850 hPa, not shown). Focus on the upper troposphere is also suggested by Suematsu and Miura (2020), who found greater association of upper-tropospheric zonal wind with MJO phase speed by other methods. This association demonstrates that although the mechanisms controlling phase speeds are uncertain, the net association of phase speed with advection by upper-tropospheric background wind is positive. That is, less upper-tropospheric easterly wind is associated with more rapid eastward propagation. Since the total effect of background wind on MJO phase speed might be different from the effect of advection alone, the conclusions of the potential relevance of advection must depend on the scale of advection assessed in this manuscript and the general association between the same advection and the background wind as already assessed by Suematsu and Miura (2020). Otherwise, careful calculation of advection alone might not account for other factors correlated with phase speed that could even result in a reversed association between advection and phase speed. This manuscript therefore assesses the scale of advection by the upper-tropospheric background wind of the MJO associated upper-tropospheric circulation. If the results correspond with those of Suematsu and Miura (2020), it would suggest that advection of the MJO circulation by

the upper-tropospheric background wind is a credible candidate for contributing substantively to variability in MJO phase speed.

2. Data and methods

Zonal wind data at 200 hPa were obtained from the ERA5 on a 1° grid with daily mean resolution. Interpolated satellite outgoing longwave radiation data were obtained from the NOAA ESRL, on a 2.5° grid (Liebmann and Smith 1996). Data are analyzed between 1979 and 2020. The long-term mean and the annual cycle and its first four harmonics are removed by a least squares fit. Background zonal wind \bar{u} is found by a 100-day low-pass filter, by means of a Fourier transform (retaining the long-term mean and seasonal cycle). Subseasonal and shorter time-scale wind u' is calculated by applying an 80-day high-pass filter to the anomaly data. All data are averaged from 10°N to 10°S after filtering, bringing the focus to the equatorial region. Advection of the subseasonal wind by the background wind is calculated following

$$adv = -\overline{u}\frac{du'}{dx} \tag{1}$$

by using centered finite differencing applied to the filtered ERA5 zonal wind data.

The algorithm applied depends on creating a longitude grid of estimates of the value of adv in the equatorial plane using (1). Next, it uses the standard simple linear regression equation for centered data,

$$y = mx, (2)$$

at each grid point in a longitudinally global grid of data y, which represents separately zonal wind data u' and the advection term (1), to find the relationship between MJO circulation signals at the selected phase speed and these target fields; x is the wavelet-filtered predictor index targeting MJO signal at a particular phase speed. The algorithm finds by regression the zonal wind anomaly u' associated with MJO circulation signal at a given phase speed, then finds the zonal gradient of the regressed result by centered finite difference. As these regressed signals evolve smoothly in space, the 1° spatial resolution of these ERA5 data are sufficient.

The estimated background wind at the base point, then, is

$$\overline{u} = \frac{-\text{adv}}{du'/dx},\tag{3}$$

and can be accurate as long as the zonal gradient of not close to zero.

Space-time wavelet analysis is used to extract the MJO circulation signal at a given phase speed. The wavelet pattern is

$$w(t,x) = \frac{1}{\sqrt{f_{bx}\pi}} \frac{1}{\sqrt{f_{bt}\pi}} \cos[2\pi(f_x x - f_t t)] \exp\left(\frac{-x^2}{f_{bx}}\right) \exp\left(\frac{-t^2}{f_{bt}}\right),$$
(4)

where f_{bx} is a longitudinal bandwidth (set at 10000); f_{bt} represents temporal bandwidth, (set at 1000); and f_x is the center

wavenumber of the wavelet, which is set to 2/360 for wavenumber 2, because that is the dominant zonal scale of MJO signals over the Indo-Pacific warm pool. Results do not depend strongly on these parameters. Finally, f_t represents the center frequency, which is defined by (5):

$$f_t = \frac{2}{2\pi R_E} \times c \times \frac{86400 \text{ s}}{\text{day}},\tag{5}$$

where R_E is the radius of Earth at the equator and c is the target phase speed. The last term in (5) converts the units of frequency to cycles per day, as that is the context of (4). A wavelet-filtered base index for regression analysis is made by centering the wavelet pattern at 80°E (near the center of strongest MJO variance in convection over the Indian Ocean) and projecting data onto it centered at each time step of the data. Many different variables could be used for the filtered base index. It is most popular to choose an index of OLR anomalies or a better tracer of rainfall. However, since the objective here is to assess the scale of advection by the background wind, the advection data estimated from (1) are used. The resulting regression analysis at the base point then exactly specifies the value of the regressed advection term, and applies separate regressions also based thereon to diagnose the scale of the zonal gradient of the intraseasonal zonal wind. If the base index were made from OLR or rainfall, the associated advection signal would maximize at some location other than the base point. In that case, solving (1) may involve occasional effective division by zero zonal wind gradient, which would radically reduce the accuracy of the result. Advection by low-frequency background wind would typically maximize amplitude at a location where the zonal gradient of intraseasonal wind is minimized or maximized, depending on the sign of the background wind. This choice thus optimizes accuracy of the conclusion, because dividing by zero zonal wind gradient will never occur given a base index defined from data estimated from (1).

The resulting regressed advection term is easily compared against regressed signals in any other variable, here including OLR anomaly, geopotential height anomaly, and zonal wind anomaly. The ultimate objective is to set the scale of the given advection term, then divide it by the corresponding negative of the zonal gradient of the regressed zonal wind at the selected phase speed (scaled to the same advection term), following (3), thereby revealing the expectation value of the background wind \overline{u} that is associated with the MJO signal at each selected phase speed. Phase speeds assessed are 3, 4, 5, and 7 m s⁻¹.

Because outlier and non-Gaussian data can affect results of least squares regression, robust regression following the Theil (1965) approach is applied here. Thiel regression splits the point cloud into the set of all pairs of points, finds the slope of the line created by each pair, then takes the median value as the result. That result provides an estimate of the slope coefficient that is robust to outliers, while the algorithm also gives a 95% confidence interval therein, which is used here for significance testing. Unfortunately, the algorithm is far more computationally intensive than ordinary least squares regression,

because large datasets will have large numbers of pairs of points, shrinking the reasonable subset of contexts considered here, and narrowing the focus to the upper troposphere, where the scale of advection will be stronger because of stronger winds observed there relative to the lower or middle troposphere. However, by focusing on a location of strongest MJO convective variance, on the central zonal scale of MJO convection over the warm pool (wavenumber 2), and on the upper troposphere where winds are strongest, the results will apply to the contexts likely most important to the MJO circulation signal and to its broader background context. Other aspects of the MJO, such as its moisture dependence, might focus in the lower troposphere where moisture concentrates.

Although the MJO varies substantially across the year, especially in terms of its meridional structure, when considered in the equatorial plane, MJO circulation events circumnavigate the world across and between all seasons. The same disturbance moving around the world would gradually express itself differently depending on the mean state at the time and place. The background zonal wind over the Indian Ocean has a substantial seasonal cycle, the range of which could not be fully expressed without including the full year in the analysis. Therefore, this analysis includes data from throughout the year. Given that the upper-tropospheric background wind over the Indian Ocean is most easterly during the Northern Hemisphere summer Indian monsoon, the contributions of zonal advection to the zonal phase speed may be strongest then.

3. Results

Longitude-time lag diagrams of regressed zonal wind and OLR anomalies are shown in Fig. 1. The center column shows the regressions based on the median slope coefficients, while the left and right columns show the results at the lower and upper bounds of the 95% confidence intervals on the regression coefficients. The top row shows results at 3 m s⁻¹, the middle row shows 5 m s $^{-1}$, and the bottom row shows 7 m s $^{-1}$. An estimate at 4 m s⁻¹ was also made but is not shown, for brevity. Shading shows OLR anomaly, with active convection suggested in blue. Contours show the regressed 200-hPa zonal wind anomaly. Reference lines drawn near the base point show 3, 5, and 7 m s⁻¹ on each diagram, and are intended for comparison against anomalies over the Indian Ocean near the base point. The lines compare best with the regressed signals in the row corresponding to the given speed, based on proximate contour lines. It is expected that with time lag and distance from the base point and lag zero, phase speed will vary from that extracted from the wavelet filter, because phase speeds of events are not constant (e.g., they tend to speed up near the date line). Each figure shows slow signal proximate to the base longitude and faster signal toward the east, but faster signals near the base point cooccur with faster speeds in regressed zonal wind anomalies near and east of the date line. This outcome is not surprising since phenomena like El Niño-Southern Oscillation that can influence background wind anomalies that simultaneously disturb wind and moisture signals around the world in correlated geographical patterns. The period of the

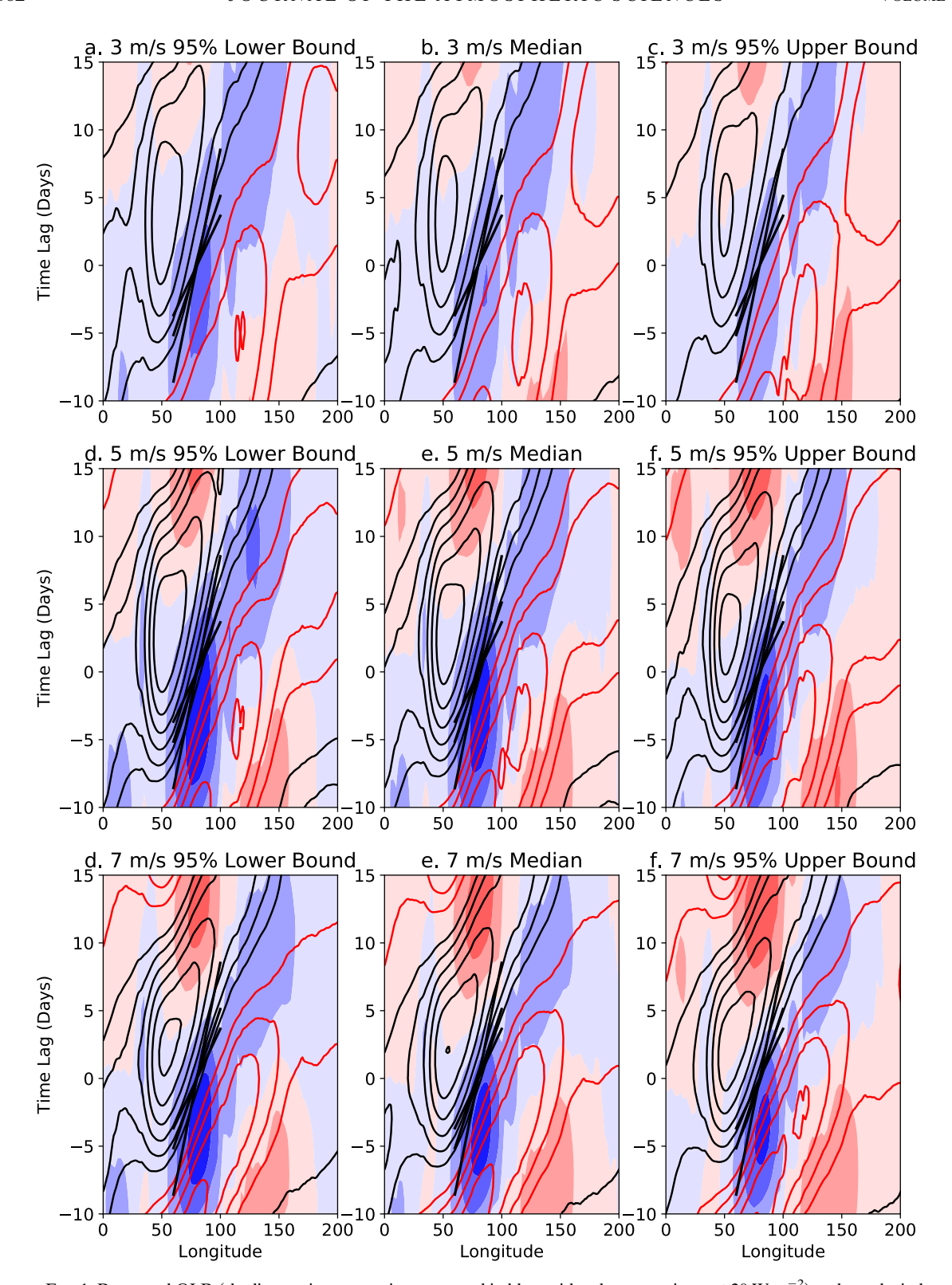


Fig. 1. Regressed OLR (shading; active convection suggested in blue, with color saturating at $\pm 20~W~m^{-2}$) and zonal wind anomaly (contours every 0.5 m s⁻¹, with the zero line omitted; red represents westerly). Results are shown for (top) 3, (middle) 5, and (bottom) 7 m s⁻¹. Columns show (left) the lower bound of the 95% confidence interval, (center) the median, and (right) the upper bound of the Theil regression slope coefficients.

TARIF 1	Advection	analysis	results
I ADLE 1.	Auvection	anarysis	icsuits.

Wavelet speed	5% confidence level	Center	95% confidence level	Speed adjusted for advection	Difference between center values
\overline{u}_3	-11.37	-13.37	-15.53	16.4	
\overline{u}_4	-9.86	-11.2	-12.58	15.2	2.17
\overline{u}_5	-9.31	-10.45	-11.64	15.5	0.75
\overline{u}_7	-9.11	-10.27	-11.46	17.3	0.18

regressed OLR and zonal wind signals is longest for the slowest signals, as anticipated, given that the wavenumber analyzed is fixed at 2.

Table 1 Background wind estimated for each wavelet phase speed (all values in m s⁻¹), including the 95% confidence interval on calculated advection. Speed adjusted for advection is the wavelet speed minus the center advection value. The difference between center values is given in rows that are between the relevant wavelet speeds.

Table 1 gives the 95% confidence intervals of the estimated associated background wind at 3, 4, 5, and 7 m s⁻¹ phase speeds at the base longitude. The center of the distribution of background winds is most easterly at the slowest analyzed speed of 3 m s⁻¹ (-13.4 m s⁻¹ background wind) and weakest easterly (10.3 m s⁻¹ background wind) at the fastest analyzed speed of 7 m s⁻¹. For the 7 m s⁻¹ phase speed, the diagnosed effect of advection on the Earth-relative phase speed is around 10 m s⁻¹ (see the column in Table 1 entitled "speed adjusted for advection"), suggesting that in the absence of the effect of advection of a wave of the same zonal scale in a hypothetical resting basic state that holds all else equal, the signal would be moving eastward at 17 m s⁻¹. The results similarly suggest that the slowest signals analyzed, at 3 m s⁻¹ would have been moving at 16.4 m s⁻¹ in the absence of advection effects in that same hypothetical resting background state, and a 4 or 5 m s⁻¹ signal would have been moving at about 15.2 or 15.5 m s⁻¹. In order for the slowest MJO signals prior to adjusting for advection to be faster than MJO signals near the frequency of the spectral maximum, these slow events must be disproportionately impacted by advection than faster signals. Although the speeds of the 3 and 4 m s⁻¹ MJO signals are only 1 m s⁻¹ apart, the difference between the implied background winds associated with the advection signal is 2.2 m s⁻¹, and given the full range of the 95% confidence interval, the true result likely lands between 1.5 and 3 times the assessed difference in phase speed. In contrast, the fastest events assessed are 2 m s⁻¹ apart, and have calculated background wind only 0.2 m s⁻¹ apart, suggesting that other factors must dominate the difference in phase speed between fast events. Nevertheless, even the fast 7 m s⁻¹ events are advected nearly 9 m s⁻¹ toward the west.

4. Conclusions

This paper assesses the direct contribution advection by upper-tropospheric background wind to MJO phase speed

over the equatorial Indian Ocean by using a robust linear regression algorithm and the definition of advection of subseasonal zonal wind by 100-day low-pass filtered 200-hPa zonal wind. Analysis of ERA5 data herein (Table 1) shows that advection by the background wind typically slows the eastward progression of 200-hPa circulation signals associated with the MJO by 9-15 m s⁻¹ (including the 95% confidence interval) as applied to MJO circulation signals observed moving eastward at from 3 to 7 m s⁻¹. The slowest MJO signals assessed are evidently affected most, suggesting that advection by the background wind helps distinguish those events as slow. Subtracting the calculated advection values approximates the speed of the disturbances in a hypothetical resting field in which all else is equal including the same zonal scale. Results show that both the slowest and fastest observed MJO signals assessed would be faster in such background conditions than events observed at 4-5 m s⁻¹. Events near 4-5 m s⁻¹ occur close to the spectral peak of OLR anomalies associated with the MJO at zonal wavenumber 2, implying that their average amplitude in tropical convection is the strongest. Absent the effects of advection, the slowest MJO events would therefore be the ones with the most intense convection. The slowest MJO events at the lowest observed MJO frequencies analyzed here experience so much advection by anomalous upper-tropospheric easterly background wind that if they instead occurred in an average background wind base state, their frequency would be higher than the MJO OLR spectral peak instead of lower. Results also suggest that advection distinguishes the phase speed of MJO signals most at the slowest speeds, while other factors must yield the differences in phase speed between faster MJO signals.

One hypothesis for future work that would be consistent with the above results is that deep convection associated with the MJO slows it down, but the potential intensity of deep convection associated with the MJO covaries with the background wind. The balance of factors leads to the strongest average amplitude of convection at 48 days. Fast MJO events, those characterized by periods shorter than 48 days, are associated with weaker average OLR anomalies, but as the frequency approaches the spectral peak (suggesting slower propagation), OLR amplitude increases. At periods longer than 48 days, in contrast, the spectrum suggests that slower MJO events are associated with weaker OLR anomalies (see the power spectrum of Wheeler and Kiladis 1999). The results shown here suggest that slow MJO events are associated with much stronger effects of easterly advection by the background wind than fast events. The structure of the spectrum and these results together suggest the hypothesis that reduced background moisture might speed up the slowest events only to be more than offset by increased effects of advection acting in the opposite direction in those events. This potential nonlinear competition between moist effects and advection by the background wind *might* explain why the spectral peak occurs where it does. Further work is required to assess the association of moist processes to MJO phase speed after controlling for background wind.

Acknowledgments. Funding was provided by National Science Foundation Grants 1757342 and 2103624 to Paul Roundy. ECMWF provided ERA5 data, and the NOAA ESRL provided interpolated satellite outgoing longwave radiation data.

Data availability statement. Data are freely available from ECMWF and the NOAA ESRL. Code to replicate the analysis is available by request from the author (please give 2 weeks for response).

REFERENCES

- Chen, G., and B. Wang, 2020: Circulation factors determining the propagation speed of the Madden–Julian oscillation. J. Climate, 33, 3367–3380, https://doi.org/10.1175/JCLI-D-19-0661.1.
- Cho, H., K. P. Bowman, and G. R. North, 2004: Equatorial waves including the Madden–Julian oscillation in TRMM rainfall and OLR data. *J. Climate*, 17, 4387–4406, https://doi.org/10. 1175/3215.1.
- Gribble-Verhagen, L., and P. E. Roundy, 2010: Analysis of apparent coupling between an oceanic Kelvin wave and atmospheric convection during the winter of 1986/87. *J. Climate*, 23, 6352–6364, https://doi.org/10.1175/2010JCLI3790.1.
- Hendon, H. H., and M. L. Salby, 1994: The life cycle of the Madden–Julian oscillation. *J. Atmos. Sci.*, **51**, 2225–2237, https://doi.org/10.1175/1520-0469(1994)051<2225:TLCOTM>2.0.CO;2.
- Hu, F., and T. Li, 2021: Effects of MJO vertically tilted structure on its phase speed from the moisture mode theory

- perspective. J. Climate, **34**, 4505–4520, https://doi.org/10.1175/ JCLI-D-20-0732.1.
- Jiang, X., E. Maloney, and H. Su, 2020: Large-scale controls of propagation of the Madden-Julian oscillation. npj Climate Atmos. Sci., 3, 29, https://doi.org/10.1038/s41612-020-00134-x.
- Liebmann, B., and C. A. Smith, 1996: Description of a complete (interpolated) outgoing longwave radiation dataset. *Bull. Amer. Meteor. Soc.*, 77, 1275–1277, https://doi.org/10.1175/1520-0477-77.6.1274.
- Madden, R. A., and P. R. Julian, 1972: Description of global-scale circulation cells in the tropics with a 40–50 day period. J. Atmos. Sci., 29, 1109–1123, https://doi.org/10.1175/1520-0469(1972)029<1109:DOGSCC>2.0.CO;2.
- Roundy, P. E., 2018: A wave-number frequency wavelet analysis of convectively coupled equatorial waves and the MJO over the Indian Ocean. *Quart. J. Roy. Meteor. Soc.*, **144**, 333–343, https://doi.org/10.1002/qi.3207.
- —, 2021: The association between the phase speed of the Madden–Julian oscillation and atmospheric circulation. *The Multiscale Global Monsoon System*, Asia-Pacific Weather and Climate Series, Vol. 11, World Scientific, 301–314, https://doi.org/10.1142/9789811216602_0024.
- Shaaban, A., 2020: On the structure and phase speed of the Kelvin waves and MJO over the Indian Ocean. Ph.D. dissertation, Dept. of Atmospheric and Environmental Sciences, University at Albany, State University of New York, 105 pp.
- Suematsu, T., 2018: A study on the background sea surface temperature field and moist processes contributing to the realization of the Madden-Julian oscillation. Ph.D. dissertation, The University of Tokyo, 119 pp.
- —, and H. Miura, 2020: Modulation of MJO propagation speed by the fluctuation of large-scale background zonal circulation. 100th AMS Annual Meeting, Boston, MA, Amer. Meteor. Soc., 368057, https://ams.confex.com/ams/2020Annual/webprogram/ Paper368057.html.
- Theil, H., 1965: The analysis of disturbances in regression analysis. *J. Amer. Stat. Assoc.*, **60**, 1067–1079, https://doi.org/10.1080/01621459.1965.10480851.
- Wheeler, M., and G. N. Kiladis, 1999: Convectively coupled equatorial waves: Analysis of clouds and temperature in the wavenumber–frequency domain. *J. Atmos. Sci.*, 56, 374–399, https://doi.org/10.1175/1520-0469(1999)056<0374:CCEWAO>2.0.CO;2.